Supraglacial weathering crust dynamics inferred from cryoconite hole hydrology

Cook, Joe; Hodson, Andrew J.; Irvine-Fynn, Tristram

Published in:
Hydrological Processes

DOI:
10.1002/hyp.10602

Publication date:
2016

Citation for published version (APA):
Cook, J., Hodson, A. J., & Irvine-Fynn, T. (2016). Supraglacial weathering crust dynamics inferred from cryoconite hole hydrology. *Hydrological Processes*, *30*(3), 433-446. https://doi.org/10.1002/hyp.10602

Supraglacial weathering crust dynamics inferred from cryoconite hole hydrology

J.M.Cook[1], A. J. Hodson[2,3] , T.D.L. Irvine-Fynn[4]

1 – College of Life and Natural Sciences, University of Derby, Derby, DE22 1GB
2 – Department of Geography, University of Sheffield, Sheffield, S10 2TN
3 – Arctic Geology, University Centre in Svalbard, Longyearbyen, Norway
4 – Centre for Glaciology, Aberystwyth University, Aberystwyth SY23 3DB.

Corresponding Author: J M Cook, j.cook1@derby.ac.uk

This article has been accepted for publication and undergone full peer review but has not been through the copyediting, typesetting, pagination and proofreading process which may lead to differences between this version and the Version of Record. Please cite this article as doi: 10.1002/hyp.10602

Introduction

Building upon work by Muller and Keeler (1969), Irvine-Fynn and Edwards (2014) examined the ecological role and significance of the "weathering crust" - the shallow (~2 m) layer of porous ice that develops seasonally over ablating glacier surfaces. They asserted that, excluding Antarctica, global glacial weathering crusts may support some 10^{21} to 10^{26} microbes (Irvine-Fynn & Edwards, 2014), representing an important yet poorly understood component of supraglacial ecosystems. Hydrological fluxes through the weathering crust may profoundly influence in situ microbial communities (Edwards et al. 2011), export of microbial cells from glacier surfaces (Irvine-Fynn et al., 2012) and biodiversity in glacier-fed streams (Wilhelm et al., 2013), making the hydrological behaviour of the weathering crust an important area of research. Despite previous researchers directing attention to supraglacial hydrology (e.g. Derikx, 1971; Munro, 2011), surprisingly little literature exists directly examining water movement through near-surface ice (e.g. Theakstone & Knudsen, 1981; Karlstrom et al. 2014).

The weathering crust forms due to subsurface melt from shortwave radiation (I*), the attenuation of which typically limits subsurface melting on glaciers to within a "photic zone" (Irvine-Fynn & Edwards, 2014) a few tens of centimetres thick (Shumskii, 1964), but can extend to greater depths defined by Beer's Law, which describes the exponential decay of solar radiation as a function of distance through ice (Oke, 1987):

$$I_z^* = I_0^* e^{-kz} \qquad \text{(Eq.1)}$$

where I^*_z is the shortwave incident radiation at depth z, I^*_0 is the radiation flux at the ice surface and k is the extinction coefficient. Values of k vary in supraglacial ecosystems (Hodson et al. 2013), but typically lie in the range 2.00 – 20.00 m^{-1} for optically clear (blue) glacier ice and dry snow respectively (Hodson et al. 2013). By contrast, the value for pure ice is ~6.00×10^{-4} m^{-1} (Geiger, 1965). The dissipation of radiative energy in the photic zone leads to subsurface melting, enlarging interstitial spaces and disaggregating ice crystals. Additionally, heat flow within the interstitial space further contributes to the declining cohesion of the near-surface ice crystals (Nye, 1991). This decaying surface has been referred to as "honeycomb ice" (e.g. Zeng et al. 1984; Cutler & Munro, 1996), and detailed energy balance studies have demonstrated the relative importance of the subsurface melt volume (see Munro, 1990; Wheler and Flowers, 2011). Near-surface ice exhibits a characteristic non-linear trend of increasing ice density with depth (LaChapelle, 1959; 1961): from a highly porous surface (300 kg m^{-3}: Shumskii, 1964; Schuster, 2001) to a dense subsurface of ~900 kg m^{-3}.

Muller & Keeler (1969) indicated a meteorological control on weathering crust evolution: maximum rates of weathering crust formation are associated with clear sky conditions that allow I* to dominate the surface energy balance. During such periods the overall porosity of the near-surface ice progressively increases, and the weathering crust expands vertically to greater depth. Consequently, through increased porosity, the weathering crust becomes a location for storage of meltwater (Larson, 1978; Liestøl et al. 1980; Irvine-Fynn et al. 2006; Irvine-Fynn, 2008), controlling near-surface drainage velocities (Wakahama et al. 1973; Larsen, 1977; Shea et al. 2005; Munro, 2011), and providing a substrate vulnerable to supraglacial rill initiation (Schuster, 2001). Recent work by Karlstom et al. (2014) connected microscale weathering crust hydraulics to macroscale supraglacial meltwater flow features and indicated a research imperative is to improve current understanding of the dynamics of sub-surface flow.

During synoptic periods of cloud cover, high air temperatures and high wind speeds, the surface energy balance can become dominated by turbulent heat fluxes. This has a three-fold effect: first, selective radiation-driven subsurface melting can decrease or stop; second, refreezing of melt water in interstitial pore spaces can occur; and third, low density surface-ice ablates through convective melting. These processes cause the weathering crust to decay rapidly (Muller and Keeler, 1969; Schuster, 2001). Energy input by rainfall may also contribute to the removal of porous weathering crust ice (Muller & Keeler, 1969), although this method of ablation is often assumed negligible

(Rothlisberger and Lang, 1987). With decreased porosity, the role of the weathering crust in hydrologic transmission and storage soon diminishes. As a depth limited aquifer, the dynamic weathering crust's dynamic impact on supraglacial hydrographs at short (sub-hourly) to seasonal time-scales is, therefore, complex and remains largely unexplored (Irvine-Fynn et al. 2011).

As highlighted by Muller and Keeler (1969) and Irvine-Fynn & Edwards (2014), the weathering crust provides the substrate for the development of cryoconite holes. These are pits with quasi-circular planforms that develop on ice surfaces worldwide due to enhanced ablation under patches of biologically inoculated sediment. They have been recognised as areas of high biodiversity and microbial activity due to the relatively stable, well-illuminated and nutrient-rich environments they offer microbes (e.g. McIntyre, 1984; Wharton, 1985; Hodson et al. 2008; Cook et al. 2010; Edwards et al. 2013a). Despite cryoconite holes traditionally being viewed as discrete microbial habitats (e.g. Wharton et al. 1985), they generally contain a column of melt water which may exhibit stratified populations of protozoa (Mieczen et al. 2013), and are likely hydrologically connected to the weathering crust aquifer. There is currently a paucity of literature concerning hydrological processes operating within cryoconite holes and their role in the wider weathering crust hydraulic regime.

To date, most research into cryoconite hole hydrology has been limited to Antarctica (e.g. Tranter et al. 2004; Fountain et al. 2004; Bagshaw et al. 2007; MacDonnell and Fitzsimons, 2008; Hodson et al. 2013) where low surface temperatures promote the formation of thick ice lids that decouple cryoconite holes from hydrological, microbiological, gaseous and sedimentological exchanges with the atmosphere and glacier surface. Critically, in Antarctica, where low air temperatures inhibit surface melting, internal subsurface melting by shortwave radiation penetration occurs due to a "solid state greenhouse effect" (Brandt and Warren, 1993; Liston et al. 1999). Weathering crust development processes here contrast to those described above, and work by Hoffman et al. (2014) suggests that this only has an appreciable impact upon glacier runoff when melt water efficiently drains through the weathering crust, else it simply refreezes in situ. Consequently, while Antarctic cryoconite holes may connect to each other via discrete subsurface conduits (MacDonnell and Fitzsimons, 2008), the subsurface drainage mechanism is likely unique to cold Antarctic glaciers (Fountain et al. 2004; Hodson et al. 2013). Contrastingly, in Arctic latitudes, cryoconite holes penetrate weathered ice at melting point and generally maintain an open interface with the atmosphere during the ablation season. This suggests that Arctic cryoconite holes probably differ in their hydrologic regime and play a different role in weathering crust hydrology than their austral equivalents. However, MacDonnell and Fitzsimons (2012) described intergranular drainage development around Antarctic cryoconite holes, suggesting some commonality in the drivers of weathering crust dynamics globally.

In Arctic settings, the lack of isolation by ice lids has been linked to different biotic communities compared with those in the Antarctic, due to frequent mixing and flushing with meltwater (Meuller and Pollard, 2004) and greater inputs of allochthonous biota (Paultier et al. 2013). Furthermore, an active supraglacial hydrological system may cause disaggregation (Takeuchi et al. 2000) and redistribution (Hodson et al. 2007; Irvine-Fynn et al. 2011) of cryoconite, influencing microbial activity (Stibal et al. 2012), cyanobacterial filament lengths and therefore cryoconite grain stability (Langford et al. 2014). However, these observations are not independent from the weathering crust, where a reduction in interstitial void spaces in increasingly dense ice establishes a gradient of decreasing hydrologic transmission of labile microbes with depth (Irvine-Fynn & Edwards, 2014). Since the weathering crust is synoptically variable, rates of storage and transmission of water and microbes likely also vary at a range of spatio-temporal scales (Irvine-Fynn et al. 2012). Therefore, coupling weathering crust and cryoconite hole hydrology to inform supraglacial microbiology is a research imperative that remains under-explored. Therefore, the aims of this study were 1) to generate a high resolution time series of hydraulic changes within the weathering crust using cryoconite holes on Austre Brøggerbreen as natural boreholes; 2) to undertake rapid slug and bail tests to determine hydraulic conductivity within the weathering crust; 3) to use these data to make inferences related to the storage and transmission of water and microbes through the weathering crust.

Field site

Field work was conducted at Austre Brøggerbreen (hereafter, AB), Svalbard (78°10'49"N, 15°30'21"E; Fig. 1A) between 9th and 31st August, 2009. Mean annual air temperatures at sea level in the locality are -6.30 °C, with warmest mean monthly temperature of 4.90 °C in July, and mean annual precipitation of 400 mm yr^{-1} (eKlima, 2012). Austre Brøggerbreen is a north-facing valley glacier located on Brøggerhalvøya, with an area of ~9 km^2. The glacier's catchment extends to ~740 m asl, with ice extending from 60 to 650 m asl, and steep slopes extend from the glacier's margin to the catchment watershed in the uppermost elevations. Since 1966, AB has exhibited an almost continuously negative mass balance of -0.60 m w.e. per year (Barrand et al. 2010) with evidence for accelerated thinning in the upper 200 m of the glacier's elevation range since ca. 1990 (James et al. 2012). These recent thinning trends have resulted in AB transitioning from a polythermal to cold-based thermal regime (Nowak & Hodson, 2014).

The cold-based glacier is characterised by an extensive supraglacial drainage system, with a number of discrete moulins descending to englacial drainage routes (Vatne, 2001; Stuart et al. 2003; Vatne & Refnes, 2003). The recent and consistently negative annual mass balances have progressively exposed unconsolidated sediments at the ice margins, including in the upper ablation and accumulation areas, which may be mobilised on to the glacier surface by snow melt and thaw (Porter et al. 2010). Such sources may supplement aeolian mineral dust deposition and provision cryoconite on AB. Contrasting cryoconite microbial communities have been identified between AB and the adjacent glaciers (Edwards et al. 2011; 2013b), and, therefore, the regional representativeness of AB is unclear. Local estimates of cryoconite loading on the adjacent glacier, Midtre Lovénbreen, by Hodson et al. (2007) suggest cryoconite concentrations of up to 10600 kg km^{-2} with discrete holes being common in the upper ablation zone. According to research at Waldermarbreen (78°40'0"N, 12°0'0"E), typical depths of the weathering crust for glaciers in this region are limited to ~1 m, with deeper ice remaining below pressure melting point even during summer months (Sobota, 2009). For further details relating to the site's glaciology, hydrometeorology and ecology, see Hagen & Saetrang (1991), Hodson et al. (1998, 2002); Barrand et al. (2010) and Edwards et al., (2011).

Methods

The primary data collection at the AB field site focused upon cryoconite hole hydrology, with ancillary data used to describe the hydrometeorology of the ice surface.

Meteorology:

At the study site, boundary layer air temperature (T_a) over the observation period was measured using 10 kΩ thermistors sheltered by a Stevenson screen, positioned 1 m above the ice surface. Thermistors were calibrated prior to installation and the Steinhart-Hart equation used to convert resistance to temperature ($r^2 = 0.9998$). In addition a Delta-T ES-2 silicon photodiode was used to measure I* (across the visible range 400-1050 nm). Data were logged at 5 minute intervals, recording averages of sample measurements made every 30 s.

Time series of cryoconite hole hydrology:

To ascertain variations in water stored within cryoconite holes associated with melt inputs or weathering crust drainage processes, records of water levels in cryoconite holes were acquired. A Delta-T DL2-e data logger was placed centrally and capacitance water level sensors installed in each of eight cryoconite holes (Fig. 1B). All monitored holes were located in ablating ice that was relatively crystallographically homogeneous, in a broadly low gradient area and far from topographical features which might have imposed specific shadowing or large-scale hydrological regimes; however, holes 7 and 8 were proximate to a small meandering supraglacial stream. Average diameter and depth for all holes over the measurement period was 103 mm and 227 mm, respectively, and the average hole water volume (V_w) was 1987 cm^3.

To monitor variations in V_w, a 'goalpost' structure (Fig. 1B) was used to instrument each cryoconite hole. Two vertical 'rig poles' were inserted into pre-drilled holes ca. 20 cm either side of each hole, and a horizontal 'crossbar' used to suspend the capacitance sensors. Submergence of the sensor resulted in reduced voltage output, which is sensitive to variations in water level with respect to the probe itself. Calibration revealed a sensor error of + 1 to -2 mm. Sensors which were dry prior to submergence output a slightly higher voltage (10 - 20 mV higher) than those which had been 'pre-wetted', indicating worst-case errors of 5 mm, independent of temperature, conductivity or ionic strength of the solution.

Water level was logged at 5-minute intervals, averaging measurements made every 30 s. At each hole at least daily manual measurements of apparent surface ablation and cryoconite hole depth were gathered and used to monitor the descent of the cryoconite hole system away from the crossbar. This data was used to correct the water level data for surface ablation. Water level sensors were also repositioned daily to ensure constant submergence despite surface lowering. The magnitude of the repositioning was recorded and the data corrected accordingly. Water levels were converted into rate of volumetric change in the cryoconite hole water between times t_1 and t_2 using Equation 2:

$$\Delta V_w = \frac{\pi {r_c}^2 (h_{wl} - h_{hole} - h_{surf})}{t_2 - t_1} \quad \text{(Eq.2)}$$

where ΔV_w = change in cryoconite hole water volume, r_c is cryoconite hole radius, and h = changes in heights of cryoconite hole water meniscus, floor, and glacier ice surface (respectively, subscripts *wl*, *hole* and *surf*) (Fig 1 B).

Hydraulic conductivity in the weathering crust:

We used so-called 'slug-and-bail' tests to establish the hydraulic conductivity (K) of the weathering crust: a common technique employed in the study of saturated porous media such as soils (e.g. Bear, 1972; Amoozegar and Warrick, 1986). These were employed at a sample set of cryoconite holes in the study area. Three slug tests and three bail tests were undertaken in separate cryoconite holes. Each test was undertaken during the morning at 10am (± 1 hour). Further slug and bail tests were also undertaken in the afternoon, however the data is omitted here due to recharge being too rapid to accurately measure. For bail tests a 100 mL syringe was used to extract water in volumes of 400 mL, 1000 mL and 1500 mL, all of which represented a complete drainage of the hole water. For slug tests water was added using a 100 mL syringe in volumes of 200 mL, 300 mL and 800 mL. Water was sourced and discarded > 10 m from the test hole to avoid influencing local hydraulic gradients. Records of ΔV_w were monitored using the capacitance sensors, as described above. Slug and bail data were used to calculate saturated hydraulic conductivity (K) at five-minute intervals using Equations 2 and 3, adapted from Bouwer and Rice (1976):

$$K = \frac{r_c^2 \log\left(\frac{Re}{rw}\right)}{2d} \cdot \frac{1}{t} \log\left(\frac{h_0}{h_t}\right) \quad \text{(Eq.2)}$$

for which:

$$\log\left(\frac{R_e}{r_w}\right) = \left[\frac{1.1}{\log\left(\frac{b}{r_w}\right)} + \frac{A + B \log\left[\frac{(D-b)}{r_w}\right]}{\left(\frac{d}{r_w}\right)}\right]^{-1} \quad \text{(Eq.3)}$$

where r_c = hole radius; R_e = radial distance over which the change in head position is dissipated in the aquifer; r_w = horizontal distance from centre of well to undisturbed aquifer; d = open well depth (equal to hole depth); h_0 = water level at t_0; h_{t1} = water level at time t_1; b = hole depth; D = aquifer depth. Terms A and B are dimensionless numbers that vary according to the length of the open section of well and r_w (Bouwer and Rice, 1976). This method was appropriate because it is applicable to both slug and bail tests for boreholes of any depth and diameter.

For cryoconite holes, $d = b$ since no screen was used. Bouwer and Rice (1976) showed that when $D >> d$, as in cryoconite holes, D has negligible impact on R_e, reporting an effective upper limit for log $((D - b)/ r_w)$ of 6. Therefore, the term log $((D - b)/r_w)$ was replaced by the value 6 in Equation 2. It is also assumed that r_w is small, given the small ΔV_w recorded in cryoconite holes, observed rapid dissipation of slug water, and lack of ΔV_w in holes close (< 5 to 20 cm) to those used for slug and bail tests. Although unknown, a value of 5 cm for r_w is conservatively estimated in this study.

Melt Modelling:

Surface ablation (mm w.e.) at the study area was modelled using Brock and Arnold's (2000) point surface energy balance model. The melt model was driven by meteorological data acquired at the field site between 9th and 31st August 2010. Vapour pressure was calculated from T_a records (see Tetens, 1930). Values for local surface ice albedo of 0.4 (after Bruland and Hagen, 2002; Hodson et al. 2008) and roughness of 0.00066m (after Arnold and Rees, 2003) were used. Optimization of this model is generally accomplished by varying albedo; however, since this is a key parameter in the development of the seasonal weathering crust we ran the model *a priori*. Due to the absence of wind speed data from AB during the observation period, records from the adjacent, and similarly oriented Midtre Lovénbreen were used.

Results

Meteorology:

Over the observation period, mean T_a and I* were 0.51 ± 2.14 °C and 198.72 ± 219.90 Wm^{-2} respectively (Fig 2A). These low values reflect the reduced solar angle and declining incident radiation as the Arctic summer approaches termination, coupled with the common occurrence of low clouds (Hanssen-Bauer et al. 1990). Of note, during clear sky conditions (between 17th and 19th August), I* rose to 1132.20 Wm^{-2} whilst T_a never rose above 8.50°C. Prior to 20th August and after 24th August, night-time T_a dropped below zero; however, from 20th to 24th August T_a remained continually positive. This period is hereafter referred to as the 'Warm Air Phase'. The Warm Air Phase coincided with a period of low I*, likely resulting from insulation by sustained synoptic cloud cover causing turbulent fluxes to dominate melt processes.

Time series of cryoconite hole hydrology:

In all eight cryoconite holes, ΔV_w showed clear diurnal fluctuations out of phase with I* and T_a (Fig. 2B). Measurements from Holes 7 and 8 ended early due to invasion by a migrating supraglacial rill. Importantly, significant linear decreases in V_w over the entire measurement period were recorded in all eight holes, with an average rate of change of -0.0060 $mm^3\ s^{-1}$ (equivalent to 0.50 mL d^{-1}) and individual coefficients of determination for linear regression models between V_w and time were between 0.73 and 0.93 (Table 1) for all except Hole 1. Since the data were corrected daily for both cryoconite hole depth and surface ablation, the linear decrease in V_w over the entire observation period is not a melt or measurement artefact.

In Hole 1 diurnal ΔV_w fluctuations were amplified during the Warm Air Phase that followed 20th August; however, this was not observed in any of the other holes. The late season amplification in ΔV_w in Hole 1 influenced the overall trend in V_w. In Hole 1 following the warm air phase, V_w changed by up to 44.45 cm^3 in 16 hours (between 477 and 493 hours into measurement period; see Fig 2B), almost four times greater than the largest fluctuation in any other hole at any time during the observation period (12.3cm^3 increase in V_w between 414 and 427 hours in Hole 3).

Following detrending of the ΔV_w records using linear regression, cross correlation was used to quantify the dominant lag times between V_w and both I* and T_a in Holes 1-6. The lag times associated with maximum positive Pearson correlation coefficients ("dominant lag") and their associated R values are shown in Table 2A. For ΔV_w and I*, the mean dominant lag was 15.18 ± 3.13 hr, while the mean dominant lag between ΔV_w at T_a was 16.04 ± 4.27 hr. Data from Holes 7 and 8 were omitted due to their

invasion by a migrating supraglacial rill. Negative correlations were evident at shorter lags (Table 2B). The strongest negative correlations were invariably greater than the maximum positive correlation for the same hole. For ΔV_w and I*, the mean lag associated with maximum negative correlation was 3.59 ± 2.69 hr and between ΔV_w and T_a it was 5.28 ± 2.87 hr. Hole 1 was considered anomalous and omitted from mean lag calculations.

For each hole ΔV_w was separated into daily increase (ΔV_w^+) and daily decrease (ΔV_w^-) identified as the rising and falling limbs of the daily hydrographs. Discounting the late-season amplified fluctuations in Hole 1, the maximum ΔV_w^+ in any hole during the measurement period was 40 cm^3 compared to an average of 116 cm^3 of ΔV_w^+ required to fill the holes to capacity and cause the meniscus of the hole water to reach the ice surface. Table 3 shows daily filling and emptying rates (i.e. rate of change of ΔV_w^+ and ΔV_w^- respectively) for each hole averaged over the measurement period. The amplified filling and draining of Hole 1 late in the measurement period caused the averages for that hole to be much higher than the others, reflected in the high standard deviation. The correlation between fill and drainage rate varied between the monitored holes across a full range from weak to strong: for Holes 1 and 8, fill and drainage rates were strongly correlated while for Holes 2-6 Pearson-correlation coefficients varied between 0.01 and 0.63 (Table 3).

In all holes, the fill and drainage rates accelerated as the season progressed (except for Hole 5, in which only ΔV_w^+ accelerated, and Hole 7 where rill invasion obscured late-season phenomena), although the analysis in Table 4 illustrates that there was considerable variability, with the acceleration best described by linear models with coefficients of determination (between 0.0014 and 0.6891) and p-values varying widely between < 0.001 and 0.86. In Hole 1 only, an exponential model better explained the acceleration in filling rates ($V_w = 0.1802e^{0.1363}t$, $r^2 = 0.82$). Interestingly, despite Hole 1 being anomalous in terms of its amplified ΔV_w after the warm air phase, it shows the highest coefficient of determination for linear models and by far the lowest p-values.

Superimposed upon ΔV_w for each hole were rapid, stochastic fluctuations and occasional high magnitude outflow events henceforth referred to as sudden drainage events (SDEs: see solid triangles in Fig.2B). These SDEs tended to occur in the morning, particularly between 6 and 9 am coinciding with sharp increases in I* and accelerated melt (Fig.2B). A total of 20 SDEs were observed, of which 14 closely followed a sharp increase in I* to > 100 Wm^{-2}. The most prominent morning SDE accounted for 61% of that day's total ΔV_w^- in just 6% of the total drainage time (this occurred late in the measurement period in Hole 1). The remaining 6 SDEs occurred late in the afternoon, also closely following large increases in I* that resulted from shifting cloud cover.

Hydraulic conductivity in the weathering crust:

Following application of slug (Fig.3A) and bail (Fig.3B) tests, ΔV_w was measured in Holes 1-3 (slug tests) and Holes 4-6 (bail tests). Slug and bail tests were undertaken between 9 and 11 am, therefore during periods of falling V_w, during the first half of the measurement period. Additional slug tests and bail tests were also carried out during the afternoon, however the rates of recharge were too great to accurately measure (due to refilling outpacing bailing and drainage outpacing addition of water) and they are omitted from analysis here. In bail tests using the 3 different extraction volumes, V_w invariably showed return periods of less than 50-minutes. For slug tests in Holes 4 and 6, V_w showed return periods of less than sixty minutes; however Hole 5 never regained its original V_w. In all holes the hydrological equilibration to both slug and bail tests were invariably non-linear and explained well by logarithmic functions.

Slug and bail data were used to calculate K (Eq. 2) for each hole at five minute resolution (Table 5). In all six holes K values responded to slug and bail tests in a non-linear fashion best described using a logarithmic curve. Average K values (K_{av}) were broadly similar between all six holes and between slug and bail tests (Table 5).

Melt Modelling:

Simulated surface melt rates for the study area, at 1 hr intervals, showed clear diurnal fluctuations in antiphase with ΔV_w (Fig 2B). The average surface melt rate was 0.29 ± 0.63 mm w.e. h^{-1}, and no overall trend was observed in this data. Radiative fluxes generally dominated the surface energy balance (contributing on average 87.4% of total melt energy) although the relative contribution of radiative and turbulent fluxes varied throughout the measurement period (Fig.2C and D). Later in the season, when synoptic cloud conditions were more variable there were several periods of turbulent flux-dominated energy balance, in particular during the Warm Air Phase (20^{th} to 24^{th} August), when cloud cover caused T_a consistently above freezing whilst I* was reduced. Comparison of the relative contribution of radiative and turbulent fluxes to surface energy balance (Fig.2D) with ΔV_w (Fig.2B) shows that higher water levels coincided with periods when turbulent fluxes had greater influence on the surface energy balance and radiative-flux dominated energy balance coincided with lower water levels. The discussion below therefore considers whether the ΔV_w antiphase with shortwave radiation flux indicated that subsurface melting by shortwave radiation controlled cryoconite hole water levels.

Discussion:

Weathering crust hydrology:

Daily increases in I* drive both surface and subsurface melt, creating gradients of increasing ice density with depth and the development of the porous near-surface weathering crust ice (Muller and Keeler, 1969; Fountain and Walder, 1998; Larson, 1978). Our modelling showed that the surface energy balance was dominated by shortwave radiation fluxes during our observation period, showing that conditions widely recognised to be conducive to subsurface melt and weathering crust development were prevalent. Water level changes should therefore provide insights into the interaction between weathering crust development and surface hydrology. Our monitoring in eight holes revealed synchronous diurnal fluctuations in ΔV_w within the weathering crust that were, surprisingly, out of phase with both I* and the melt rate. Therefore, during the night, lower I* enabled refreezing and contraction of interstitial pore spaces, greater flow-impedance and greater V_w. Twelve of the fifteen hour lag between I* and ΔV_w were therefore likely to be explained by diurnal cycles of irradiance, whilst the remainder most likely represented the time taken for I* to remove the cold content of the near surface ice and cause internal melting in the weathering crust. This was well-supported by stronger negative correlations at shorter lags (Table 3) which indicated outflow induced by periods of subsurface melting during periods of greater shortwave radiation receipt. A major perturbation to the conditions described above occurred during the warm air phase, when turbulent heat fluxes dominated the surface energy balance and a general increase in ΔV_w in all cryoconite holes was observed (Fig 2B). This change was entirely consistent with weathering crust decay which has commonly been associated with turbulent-heat dominated energy balance, in contrast to periods of weathering crust growth which are associated with periods of radiative-flux dominated energy balance (Muller and Keeler, 1969; Schuster, 2001).

Coupling between cryoconite hole and weathering crust hydrology was characterised by non-linear 'overburdened' responses to slug and bail tests that suggested transmission through a saturated porous medium. The re-equilibration rate declined as ΔV_w approached its pre-perturbation value, indicative of a diminishing local hydraulic gradient. Furthermore, Hole 5 never regained pre-perturbation ΔV_w following slug testing, which may have resulted from a rise in the weathering crust water table coinciding with the slug test. Fluctuations in ΔV_w therefore likely reflected changes in the hydrologic regime of the glacier's weathering crust. Our observations of ΔV_w therefore suggested daily cycles of storage and transmission within the weathering crust, with enhanced storage at night and enhanced transmission during the day, consistent with diurnal cycles of weathering crust growth and decay. Daily ΔV_w^+ generally outpaced ΔV_w^-, suggesting storage of water at hourly-daily timescales. Slug tests showed return times of 15-60 mins, while bail tests re-equilibrated faster (15-40 mins), supporting short term hydrological storage in the weathering crust.

K values were also broadly similar between all cryoconite holes, indicating relatively uniform weathering crust permeability beyond the plot scale. In this study, data from slug and bail tests undertaken late in the day were omitted due to return times being too rapid to accurately measure, which further indicated the diurnal changes in weathering crust development through pore space change. The K values presented here were comparable to results from other glaciers, although published values vary between 14.4 cm hr^{-1} in deeply weathered, fast-flowing glacier ice (Fountain and Walder, 1998) and 1.4×10^{-6} cm hr^{-1} in slow-moving ice, controlled by deformation at the scale of individual crystals (Lliboutry, 1971). Therefore, local ice physics and crystallography appear to be important controls upon weathering crust hydrology.

A seasonal linear tend of decreasing V_w was common to all eight monitored holes (Table 1). This was not thought to be a melt artefact since surface ablation and hole-floor melt were corrected for. The linearity of the seasonal reduction in V_w suggested glacier-wide shifts in hydraulic gradient, because if local processes dominated, hydraulic overburden would likely cause non-linear re-equilibration (as demonstrated by slug and bail tests). Sobota (2009) also showed that, as might be expected, the zero degree isotherm was at its deepest during late summer conditions on Waldemarbreen (Svalbard). Therefore, if propagation of the zero-degree isotherm is driven by a dominance of I* over sensible heat supply (as was the case in the present study), then energy balance conditions can sustain a seasonal increase in weathering crust thickness. The water storage potential and permeability of near-surface ice can therefore increase accordingly, although Irvine-Fynn (2008) and Shea et al. (2005) note that this might be partially countered by refreezing at depth during periods of reduced I*. Progressive deepening of the weathering crust over the observation period almost certainly explained the linear decrease in V_w in its cryoconite holes.

Sudden Drainage Events

Punctuating daily ΔV_w^- data were SDEs. These sudden discharge events accounted for an average of 39.6% (range 10 - 94%) of the net daily outflow in an average of 8.3% (range 0.5 - 54%) of the total drainage time. A possible explanation was thermal cracking (Sanderson, 1978) or creep and fracture (Schulson and Duval, 2009) of the hole floor. Thermal stresses can become appreciable in the top 3 m of glacier ice and so cracking was linked to variations in the water tables of ice-lidded cryoconite holes upon the East Antarctic Ice Sheet (Hodson et al. 2013). However, we suggest that the more modest temperature fluctuations in Svalbard made cracking less likely and instead promote rapid adjustments in the distribution of void spaces within the near-surface ice matrix. Since SDEs synchronised closely with sudden, large increases in I*, light-driven forcing of pore aperture adjustment seems plausible in combination with any thermal cracking events that do occur. Several SDEs occurred simultaneously in different holes (or in very close succession), but were not coincident with maximum ΔV_w in the holes. Therefore forcing by energy balance conditions seemed more plausible than a hydro-fracturing process.

Our data therefore demonstrated how cryoconite holes act as natural piezometers and thus serve as indicators of weathering crust hydrology and near-surface ice processes. Our measurements of ΔV_w in cryoconite holes indicated diurnal and seasonal cycles of hydrological storage and drainage efficiency coupled to weathering crust growth and decay. During colder periods when interstitial pores refreeze and contract the weathering crust may provide longer term hydrological storage, especially when insulated beneath ice lids or seasonal snow.

Residence of cryoconite in the weathering crust

Cryoconite holes also represent discrete units of supraglacial sediment storage within the weathering crust. Movement of individual cryoconite granules through weathered ice was previously studied by Irvine-Fynn et al. (2011) who found little evidence of significant cryoconite mass transfer resulting from weathering crust hydrology on a Svalbard glacier surface, providing a context for the discussion of residence times for granules in cryoconite holes.

Since cryoconite grain diameters are probably far in excess of interstitial pore apertures, transport of cryoconite granules through hole walls was considered unlikely. The Hjulstrom-Sundborg curve (Hjulstrom, 1935; Sundborg, 1956) was used to calculate a critical flow velocity of 114 cm hr^{-1} required to entrain the average granule measured in this study (mean diameter = 0.23 mm (n=15), density = 2.61 g

cm^{-3}; source data not shown here). Given that K values showed a mean permeability of ice surrounding cryoconite holes of 0.26 cm hr^{-1} for normal flow, and a maximum of 0.65 cm hr^{-1} during the most intense SDE, threshold competence for entrainment of cryoconite was very unlikely, especially since our estimated critical entrainment velocity does not account for packing density nor the cohesive properties of biotic and biogenic material surrounding cryoconite grains. Therefore movement of granules within the hole was unlikely to occur unless the melting rate of the floor became heterogeneous and created a slope.

Furthermore, no cryoconite holes in this study overfilled at any time during the measurement period, despite changes in I* and ablation. Throughout the season, for all holes except Hole 1 (which demonstrated anomalous, amplified variations) ΔV_w was less than 40 cm^3, compared to an average ΔV_w of 116 cm^3 required to fill cryoconite holes to capacity. This implied that even if grains were entrained into suspension, redistribution onto the ice surface was very unlikely. Even at maximum ΔV_w in Hole 1, a further 75.3 cm^3 of water was required to fill the hole. This illustrates that cryoconite holes represent persistent stores of sediment within the weathering crust, making the importance of biological processes within the granule (e.g. Cook et al. 2010) less surprising. Furthermore, in the event of overtopping and redistribution of granules out of holes onto the ice surface, Irvine-Fynn et al. (2011) suggested that continued transport down-glacier would also be slow.

Melt water inundation has been implicated in the literature as a mechanism of sediment evacuation from cryoconite holes (e.g. Swan, 1992); however evidence here suggested overtopping of cryoconite holes, and by extension removal of sediment by melt water, to be very infrequent (Takeuchi et al. 2010) especially since these data represented mid-late summer melt. This supports previous assertions of multi-year residence times for sediment in cryoconite holes (e.g. Hodson et al. 2007; Anesio et al. 2009; 2010; Takeuchi et al. 2010). Exceptions may include invasion of cryoconite holes by supraglacial streams which erased Holes 7 and 8 in this study.

Microbial mobility through the weathering crust

Irvine-Fynn and Edwards (2012) showed microbial cells, organic and inorganic nutrients are transported through the weathering crust by melt water. Here, we have shown that hydrological processes have the capacity to induce size-selectivity in the transport of particulate material and associated microorganisms. We have also shown that the hydraulic conditions influence the rate of meltwater and therefore aqueous nutrient propagation through the weathering crust. Transport of microbes through the weathering crust probably therefore exposes them to varying light and nutrient conditions, influencing ecosystem structure and function (Edwards et al. 2011; 2013a; 2014). Data presented here, therefore, suggests daily and seasonal evolution of weathering crust permeability controls storage and transmission of microbes and nutrients. Microbial community structure and function may be depth-dependent, with greater I* near the ice surface associated with photo-protective pigmentation and high rates of photosynthesis, and low I* at depth more likely associated with low-light adaptation and a tendency towards net heterotrophy (e.g. Hodson et al. 2013). Studies of ciliates in cryoconite hole water found distinct stratification of species with depth in the water column, suggesting that microscale heterogeneity in biotic and abiotic conditions with depth influence microbial communities, and further indicating potential for hydrologic transmission of living cells (Irvine-Fynn and Edwards, 2014). Since redistribution of microbes between micro-environments is hydrologically controlled, weathering crust hydraulics likely influence supraglacial microbial community structure and function. Consequently, spatiotemporal heterogeneity in hydraulic transmission in the weathering crust should be explored in the context of nutrient and biomass delivery to downstream ecosystems.

Being semi-persistent sediment stores, cryoconite holes are crucial habitats for life in the weathering crust. Cryoconite holes could provide multiyear storage under favourable conditions for photosynthesis (Cook et al. 2010), abundant nutrient supply from both autochthonous and allochthonous sources, and respite from redistribution through the weathering crust, especially when cells become incorporated into cryoconite aggregates. Cryoconite holes therefore represent sites of enhanced microbial activity, storage and nutrient transformation within the weathering crust. Prolonged residence times are associated with stability and extended periods of net carbon fixation on Arctic ice surfaces (Hodson et al. 2007; Anesio et al. 2009;

Cook et al. 2012) resulting in larger, more robust cryoconite aggregates (Langford et al. 2014). This suggests cell fluxes into cryoconite holes may be important for determining surface albedo and supraglacial carbon cycling.

Fluxes of cells out of cryoconite holes may also be important for supraglacial microbial dynamics. Export of cells and dissolved nutrients is much more likely than cryoconite sediment due to the critical competence for entrainment being far lower and the possibility for passage through interstitial pores. Residence times for cells in cryoconite holes likely depends upon their incorporation into cryoconite aggregates, degree of sheltering by layers of packed grains and the occurrence of SDEs. Enhanced flow competence during SDEs might play an important role in mobilizing cells from storage in cryoconite holes. Studies of fluvial ecology in other environments (e.g. Resh et al. 1988; Reice et al. 1990, Reice, 1994; Lake, 2000) suggest that disturbance, even below critical competence, can be a primary control upon benthic ecosystem structure and function. This implies that the storage and release of cells from cryoconite sediment is also tightly coupled with weathering crust hydraulic regime. This is supported by growth rings in cryoconite cross-sections identified by Takeuchi et al. (2010) that suggest multi-year (average 3.5 year) persistence of cryoconite organic matter prior to melt-water disturbance. Similarly, Stibal et al. (2012) showed cryoconite granule size on the Greenland ice sheet to be coupled with surface slope (a proxy for runoff velocity), implying periodic biomass removal by melt water disruption. In general, cryoconite holes in flat, stable ice in the interior zones of large glaciers and ice sheets probably provide more robust stores of biota than dynamic, rapidly melting ice in small glaciers and ice-sheet margins. Langford et al. (2014) further found cryoconite aggregates in the interior of Longyearbreen (Svalbard) to be smaller than at the sides due to enhanced hydraulic erosion by concentrated flow in a central tract. Our data therefore adds to a growing literature supporting the importance of weathering crust dynamics for supraglacial ecology, both as a medium for hydrologic transfer of cells and as a substrate for cryoconite hole formation.

Conclusions:

Data from Austre Brøggerbreen described the mobility of water through the weathering crust and confirmed that its behaviour is analogous to a shallow perched aquifer. Cryoconite holes were used as natural piezometers to obtain time series of hydraulic changes within the aquifer, revealing a positive correlation between radiative forcing of melt and drainage efficiency, and therefore a negative correlation between radiation and hydrological storage and sometimes resulting in sudden drainage events (SDEs). This was suggested to result from the contraction and dilation of interstitial pores due to radiative forcing of night time refreezing and day time melting. A linear decrease in water levels in cryoconite holes was also observed and attributed to the deepening of the weathering crust over the 3-week measurement period. Cryoconite holes were shown to represent sites of prolonged cryoconite storage, which explains why they are loci of enhanced microbial activity and biogeochemical cycling. Complex relationships therefore likely exist between weathering crust growth and decay, environmental stresses, microbial activity and hydraulic redistribution of nutrients and biomass. This study highlights the dynamic weathering crust as a crucial component of the hydrology, microbial ecology and biogeochemistry of the glacier ecosystem and glacierised regions.

Acknowledgements:

J. Cook acknowledges his UK National Environment Research Council (NERC) Doctoral Training Grant (No. NE/G524152/1). A Edwards and M Sweet are thanked for helpful comments on draft manuscripts.

References:

Amoozegar A, Warrick AW. 1986. Hydraulic conductivity in saturated soils: field methods. In Klute, A (Ed) Methods of Soil Analysis pt. 1, American Society of Agronomy, WI. pp.735-798.

Anesio AM, Hodson AJ, Fritz A, Psenner R, Sattler B. 2007. High microbial activity on glaciers: importance to the global carbon cycle, *Global Change Biology*, 15 (4): 955-960.

Anesio AM, Sattler B, Foreman C, Telling J, Hodson A, Tranter M, Psenner R. 2010. Carbon fluxes through bacterial communities on glacier surfaces, *Annals of Glaciology, 51 (56): 32-40*.

Arnold NS, Rees WG. 2003. Self-similarity in glacier surface characteristics, *Journal of Glaciology,* 49, 547–554, doi:10.3189/172756503781830368.

Bagshaw EA, Tranter M, Fountain AG, Welch KA, Basagic H, Lyons WB. 2007. Biogeochemical evolution of cryoconite holes on Canada Glacier, Taylor Valley, Antarctica, *Journal of Geophysical Research,* 112, G04S35.

Barrand NE, James TD, Murray T.2010. Spatiotemporal variability in elevation changes of two high-Arctic valley glaciers. *Journal of Glaciology* 56 (199): 771–780.

Bear J. 1972. Dynamics of Fluids in Porous Media. Dover Publications. ISBN 0-486-65675-6.

Bouwer H, Rice RC. 1976. A slug test for determining hydraulic conductivity of unconfined aquifers with completely or partially penetrating wells. *Water Resources Research*, 12 (3): 423-428.

Brandt RE, Warren SG.1993. Solar-heating rates and temperature profiles in Antarctic snow and ice, *Journal of Glaciology*, 39 (131): 99 – 110.

Brock BW, Arnold NS. 2000. A spreadsheet-based (Microsoft Excel) point surface energy balance model for glacier and snow melt studies. *Earth Surface Processes and Landforms,* 25: 649–658.

Bruland O, Hagen JO. 2002. Glacial mass balance of Austre Brøggerbreen (Spitsbergen) 1971-1999, modelled with a precipitation-runoff model. *Polar Research,* 21 (1): 109-121.

Cook J, Hodson A, Telling J, Anesio AM, Irvine-Fynn T, Bellas C. 2010. The mass–area relationship within cryoconite holes and its implications for primary production. *Annals of Glaciology,*51 (56): 106-110.

Cook JM, Hodson AJ, Anesio AM, Hanna E**,** Yallop M, Stiba, M, Telling J, Huybrechts P. 2012. An improved estimate of microbially mediated carbon fluxes from the Greenland Ice Sheet. *Journal of Glaciology*, 58(212), 1098–1108.

Cutler PM, Munro DS. 1996. Visible and near-infrared reflectivity during the ablation period on Peyto Glacier, Alberta, Canada. *Journal of Glaciology*, 42 (141): 333-340.

Derikx L. 1971. The heat balance and associated runoff from an experimental site on the glacier tongue, *International Association of Scientific Hydrology Publication*, 104, 59–69.

Edwards A, Anesio AM, Rassner SM, Sattler B, Hubbard B, Perkins WT, Young M, Griffith GW. 2011. Possible interactions between bacterial diversity, microbial activity and supraglacial hydrology of cryoconite holes in Svalbard. *The ISME Journal,* 5: 150-160.

Edwards A, Pachebat JA, Swain M, Hegarty M, Hodson A, Irvine-Fynn TDL, Rassner SM, Sattler B. 2013a. A metagenomic snapshot of taxonomic and functional diversity in an alpine glacier cryoconite ecosystem. *Environmental Research Letters,* 8 (035003): 11pp.

Edwards, A, Rassner SM, Anesio AM, Worgan HJ, Irvine-Fynn TD, Williams HW, Sattler B, Griffith GW. 2013b. Contrasts between the cryoconite and ice-marginal bacterial communities of Svalbard glaciers. *Polar Research,* 32, DOI: 10.3402/polar.v32i0.19468.

Edwards A, Mur L, Girdwood S, Anesio A, Stibal M, Rassner S, Hell K, Pachebat J, Post B, Bussell J, Cameron S, Griffith G, Hodson A. 2014. Coupled cryoconite ecosystem structure-function relationships are revealed by comparing bacterial communities in Alpine and Arctic glaciers. *FEMS Microbial Ecology,* Doi: 10.1111/1574-6941.12283.

Fountain AG, Walder JS. 1998. Water flow through termperate glaciers. *Reviews of Geophysics,* 36 (3): 299-328.

Fountain AG, Tranter M, Nylen TH, Lewis KJ, Meuller DR. 2004. Evolution of cryoconite holes and their contribution to meltwater runoff from glaciers in the mcMurdo Dry Valleys, Antarctica. *Journal of Glaciology*, 50 (168): 35-45.

Geiger R. 1965. Das Klima der bodennahen Luftschicht. Vierte Auflage. Braunschweig, Friedrich Vieweg und Sohn. [English translation: The climate near the ground. Translated by Scripta Technica, Inc. Cambridge, Mass., Harvard University Press, 1965.]

Hagen JO, Sætrang A. 1991. Radio-echo soundings of sub-polar glaciers with low frequency radar. *Polar Research*, 9: 99-107.

Hanssen-Bauer I, Kristensen-Solis M, Steffensen EL. 1990. The climate of Spitsbergen. (Det Norske Meteorologiske Institutt) *DNMI Klima Rapp.* 39.

Hjulstrom F. 1935. Studies of the morphological activity of rivers as illustrated by the river Fyris. *Bulletin of Geology, Institute of Uppsala*, 25: 221-527.

Hodson AJ, Gurnell AM, Washington R, Tranter M, Clark MJ, Hagen JO. 1998. Meteorological and runoff time-series characteristics in a small, high-Arctic glaciated basin, Svalbard. *Hydrological Processes*, 12 (3): 509–526.

Hodson A, Tranter M, Gurnell A, Clark M, Hagen JO. 2002. The hydrochemistry of Bayelva, a high Arctic proglacial stream in Svalbard *Journal of Hydrology*, 257: 91-114.

Hodson AJ, Anesio AM, Ng F, Watson R, Quirk J, Irvine-Fynn T, Dye A, Clark C, McCloy P, Kohler J, Sattler B. 2007. A glacier respires: Quantifying the distribution and respiration CO_2 flux of cryoconite across and entire Arctic supraglacial system. *Journal of Geophysical Research, 112 (G04S36), doi: 10.1029/2007JG000452.*

Hodson AJ, Anesio AM, Tranter M, Fountain AG, Osborn M, Priscu J, Laybourn-Parry J, Sattler B. 2008. Glacial Ecosystems, *Ecological Monographs*, 78 (1), 41-67.

Hodson A, Paterson H, Westwood K, Cameron K, Laybourn-Parry J. 2013. A blue-ice ecosystem on the margins of the East Antarctic ice sheet. *Journal of Glaciology*, 59 (214): 255-268.

Hoffman MJ, Fountain AG, Liston GE. 2014. Near surface internal melting: a substantial mass loss on Antarctic Dry Valley glaciers. *Journal of Glaciology,* 60 (220): 361-374.

Irvine-Fynn TDL, Moorman BJ, Williams JLM, Walter FSA. 2006. Seasonal changes in ground-penetrating radar signature observed at a polythermal glacier, Bylot Island, Canada. *Earth Surface Processes and Landforms,* 31: 892–909.

Irvine-Fynn TDI. 2008. Modelling runoff from the maritime arctic cryosphere: water storage and routing at Midtré Lovénbreen. *PhD thesis, University of Sheffield, 2008*

Irvine-Fynn TDL, Hodson AJ, Moorman BJ, Vatne G, Hubbard AL. 2011. Polythermal Glacier Hydrology: A review, *Reviews of Geophysics*, 49, RG4002.

Irvine-Fynn TDL, Edwards A, Newton S, Langford H, Rassner SM, Telling J, Anesio AM, Hodson AJ. 2012. Microbial cell budgets of an Arctic glacier surface quantified using flow cytometry. *Environmental Microbiology, 14 (11): 2998-3012.*

Irvine-Fynn TDL, Edwards AE. 2014. A frozen asset: The potential of flow cytometry in constraining the glacial biome. *Cytometry Part A, 85 (1): 3-7.*

James TD, Murray T, Barrand NE, Sykes HJ, Fox AJ, King MA. 2012. Observations of enhanced thinning in the upper reaches of Svalbard glaciers. *The Cryosphere*, 6 (6). 1369-1381.

Karlstrom L, Zok A, Manga M. 2014. Near-surface permeability in a supraglacial drainage basin on the Llewellyn Glacier, Juneau Icefield, British Columbia. *The Cryosphere*, 8, 537-546.

LaChapelle E.1959. Annual mass and energy exchange on the Blue glacier. *Journal of Geophysical Research.* 64: 443–9.

LaChapelle E.1961. Energy exchange measurements on the Blue Glacier. *International Association of Scientific Hydrology,* 54: 302-310.

Lake PS. 2000. Disturbance, patchiness and diversity in streams. *Journal of the North American Benthological Society*, 19 (4): 573-592.

Langford HJ, Irvine-Fynn TDL, Edwards A, Banwart SA, Hodson AJ. 2014. A spatial investigation of the environmental controls over cryoconite aggregation on Longyearbreen glacier, Svalbard, *Biogeosciences Discuss., 11, 3423-3463*.

Larson GJ. 1977. Internal drainage of stagnant ice: Burroughs Glacier, Southeast Alaska, *Institute of Polar Studies Report 65*. Ohio State University, Columbus, Ohio, pp. 33.

Larson GJ. 1978. Meltwater storage in a temperate glacier, Burroughs Glacier, Southeast Alaska. *Institute of Polar Studies Report 66*. Ohio State University, Columbus, Ohio, pp. 56.

Liestøl O, Repp K, Wold B. 1980. Supra-glacial lakes in Spitsbergen, *Norsk Geografisk Tidsskrift,* 34, 89–92.

Liston GE, Winther JG, Bruland O, Elvehoy H, Sand K. 1999. Below-surface ice melt on the coastal Antarctic ice sheet, *Journal of Glaciology,* 45 (150): 273-285.

Lliboutry LA. 1971. Permeability, brine content and temperature of temperate ice. *Journal of Glaciology,* 10 (58): 15-29.

MacDonnell S, Fitzsimons S. 2008. The formation and hydrological significance of cryoconite holes. *Progress in Physical Geography,* 32 (6): 595-610.

MacDonnell S, Fitzsimons S. 2012. Observations of cryoconite hole system processes on an Antarctic glacier. *Revista Chilena de Historia Natural,* 85: 393-407

McIntyre NF. 1984. Cryoconite hole thermodynamics. *Canadian Journal of Earth Science,* 21 (2): 152-156.

Mieczan T, Gorniak D, Swiatecki A, Zdanowski M, Tarkowska-Kukuryk M, Adamczuk M. 2013. Vertical microzonation of ciliates in cryoconite holes in Ecology Glacier, King George Island. *Polish polar Research,* 34 (2): 201-212.

Mueller DR, Pollard WH. 2004. Gradient analysis of cryoconite ecosystems from two polar glaciers, *Polar Biology,* 27, 66–74.

Muller F, Keeler CM. 1969. Errors in short-term ablation measurements on melting ice surfaces. *Journal of Glaciology,* 8 (52): 91-105.

Munro DS. 1990. Comparison of melt energy computations and ablatometer measurements on melting ice and snow. *Arctic and Alpine Research,* 22(2), 153–162.

Munro DS. 2011. Delays of supraglacial runoff from differently defined microbasin areas on the Peyto Glacier. *Hydrological Processes,* 25 (19): 2983-2994.

Nowak A, Hodson A. 2014. Changes in meltwater chemistry over a 20-year period following a thermal regime switch from polythermal to cold-based glaciation at Austre Brøggerbreen, Svalbard. *Polar Research,* 33. DOI: 10.3402/polar.v33.22779

Nye JF. 1991. The rotting of temperate ice. *Journal of crystal growth,* 113 (3-4): 465-476.

Oke TR. 1987. Boundary layer climates. Second edition. *London, Routledge Press.* 1987.

Paultier BG, Dubnick A, Sharp M, Simpson AJ, Simpson MJ. 2013. Comparison of cryoconite organic matter composition from Arctic and Antarctic glaciers at the molecular level. *Geochimica et Cosmochimica Acta,* 104: 1-18.

Porter PR, Vatne G, Ng F, Irvine-Fynn TDL.2010. Ice-marginal sediment delivery to the surface of a high-arctic glacier: Austre Broggerbreen, Svalbard. *Geografiska Annaler: Series A, Physical Geography,* 92A (4), pp. 437-449.

Reice SR, Wissmar RC, Naiman RJ. 1990. Disturbance regimes, resilience and recovery of animal communities and habitats in lotic systems. *Environmental Management,* 14 (5): 647-659.

Reice SR. 1994. Nonequilibrium determinants of biological community structure. *American Scientist,* 82: 424-435.

Resh VH, Brown AV, Covich AP, Gurtz ME, Li HW, Minshall GW, Reice SR, Sheldon AL, Wallace JB, Wissmar RC. 1988. The role of disturbance in stream ecology. *Journal of the North American Benthological Society*, 74 (4): 433-455.

Rothlisberger H, Lang H. 1987. Glacial hydrology. In Gurnell, A.M. and M.J. Clark, eds. Glacio-fluvial sediment transfer: an alpine perspective. Chichester, etc., Wiley, 207–284.

Sanderson TJO. 1978. Thermal stresses near the surface of a glacier. *Journal of Glaciology*, 20 (83): 257–283.

Schulson EM, Duval P. 2009. Creep and fracture of ice. Cambridge University Press, Cambridge, UK.

Schuster CJ. 2001. Weathering crust processes on melting glacier ice (Alberta, Canada). Theses and Dissertations (Comprehensive), Wilfred Laurier University, Paper 489.

Shea JM, Anslow FS, Marshall SJ. 2005. Hydrometeorological relationships on Haig Glacier, Alberta, Canada. *Annals of Glaciology*, 40: 52-60.

Shumskii PA. 1964. Principles of structural glaciology: the petrography of fresh-water ice as a method of glaciological investigation. Dover Publications, 497pp.

Sobota I. 2009. The near-surface ice thermal structure of the Waldemarbreen, Svalbard. *Polish Polar Research*, 30 (4): 317-338.

Stibal M, Telling J, Cook J, Man Mak K, Hodson A, Anesio A. 2012. Environmental controls upon microbial abundance on the Greenland ice sheet: a multivariate analysis approach. *Microbial Ecology*, 63: 74-84.

Stuart G, Murray T, Gamble N, Hayes K, Hodson AJ. 2003. Characterization of englacial channels by ground-penetrating radar: An example from Austre Broggerbreen, Svalbard. *Journal of Geophysical Research-Solid Earth*, 108 (B11, 2525): 13 pp.

Sundborg A. 1956. The River Klarålven: The morphological activity of flowing water erosion of the stream bed. *Geografiska Annaler*, 38: 165-221.

Swan L. 1992. The aeolian biome. *Bioscience*, 42 (4): 262-270.

Takeuchi N, Kohshima Y, Seko K, Fujita K. 2000. Characteristics of cryoconite holes on a Himalayan glacier, Yala Glacier central Nepal. *Bulletin of Glaciological Research*, 17: 51-59.

Takeuchi N, Nishiyama H, Li Z. 2010. Structure and formation process of cryoconite granules on Ürümqi glacier No. 1, Tien Shan, China. *Annals of Glaciology*, 51 (56): 9-14.

Tetens O. 1930. Uber einige meteorologische Begriffe, *Z. Geophys.* 6: 297 –309.

Theakstone WH, Knudsen NT. Dye tracing tests of water movement at the glacier Austre Okstindbreen, Norwary. *Norsk Geografisk Tidsskrift*, 35: 21-28.

Tranter M, Fountain AG, Fritsen CH, Berry-Lyons W, Priscu JC, Statham PJ, Welch KA. 2004. Extreme hydrochemical conditions in natural microcosms entombed within Antarctic ice. *Hydrological Processes*, 18: 379–387.

Vatne G. 2001. Geometry of engalcial water conduits, Austre Brøggerbreen, Svalbard. *Norsk Geografisk Tidsskrift*, 55: 24-33.

Vatne G, Refsnes I. 2003. Channel pattern and geometry of englacial conduits. *Proceedings 6th Internatinoal Symposium: Glacier caves and karst in Polar regions*. 181-188 pp.

Wakahama G, Kuroiwa D, Kobayashi D, Tanuma K, Endo Y, Mizuno Y, Kobayashi S.1973. Observations of permeating water through a glacier body, *Low Temperature Science*, 31A, 209–220.

Wharton RA, McKay CP, Simmons GM, Parker BC. 1985. Cryoconite holes on glaciers. *Bioscience*, 35: 449-503.

Wheler BA, Flowers GE. 2011. Glacier subsurface heat flux characterizations for energy balance modelling in the Donjek Range, southwest Yukon, Canada. *Journal of Glaciology*, 57 (201): 121-133.

Wilhelm L, Singer GA, Fasching C, Battin TJ, Besemer K. 2013. Microbial biodiversity in glacier-fed streams. *ISME Journal*, 7: 1651 – 1660.

Zeng Q, Cao M, Feng X, Liang F, Chen X, Sheng W. 1984. A study of spectral reflection characteristics for snow, ice and water in the north of China, in: Hydrological Applications of Remote Sensing and Remote Data Transmission, edited by: Goodison, B. E., IAHS, 145, 451–462.

Hole	Equation	r^2 value
1	V_w = -0.0004t + 0.4498	0.21
2	V_w = -0.0003t - 1.6185	0.73
3	V_w = -0.0005t - 1.4809	0.78
4	V_w = -0.0003t – 2.3209	0.74
5	V_w = -0.0004t – 0.7453	0.79
6	V_w = -0.0005t - 0.5904	0.85
7	V_w = -0.0009t - 0.4547	0.93
8	V_w = -0.0006t – 1.3092	0.75

Table 1: linear regression coefficients for seasonal scale decrease in V.

A	T_a		IR	
Hole	**Lag**	**R**	**Lag**	**R**
1	8.67	0.49	11	0.49
2	18.67	0.42	17.25	0.37
3	19.17	0.14	17.5	0.18
4	13.67	0.39	12	0.48
5	19.83	0.21	18.58	0.24
6	16.25	0.22	14.75	0.34
Mean	16.04	0.31	15.18	0.35
σ	4.27	0.14	3.13	0.12
B	T_a		IR	
Hole	**Lag**	**R**	**Lag**	**R**
1	-3.08	-0.44	0.17	-0.56
2	6.67	-0.33	5.25	-0.53
3	8.50	-0.33	7.17	-0.25
4	1.67	-0.42	1.00	-0.55
5	6.67	-0.19	6.08	-0.27
6	2.92	-0.45	1.92	-0.49
Mean	5.28	-0.36	3.59	-0.44
σ	2.87	-0.099	2.69	-0.14

Table 2: A) Lag times (hours) at which the maximum positive correlation coefficient was observed, and the Pearson correlation coefficient (R) at that lag time, for each of Holes 1 – 6. Two-tailed t-tests invariably revealed significance at $p<0.0001$.B) Lag times (hours) at which the maximum negative correlation coefficient was observed, and the Pearson correlation coefficient (R) at that lag time, for each of Holes 1-6. Two-tailed t-tests invariably revealed significance at $p<0.0001$

Hole	Fill rate ($mm^3 s^{-1}$)	σ	Drainage rate ($mm^3 s^{-1}$)	σ	R
1	22.03	21.66	-29.34	24.76	0.88
2	7.50	5.57	-8.11	4.37	0.44
3	4.02	2.95	-5.48	4.79	0.19
4	5.14	4.62	-6.21	4.41	0.01
5	3.69	4.51	-3.99	1.62	0.19
6	2.14	1.98	-2.62	1.84	0.63
7	2.48	2.15	-2.48	0.64	0.56
8	1.06	3.25	-1.26	3.92	0.81

Table 3: Measurement-period average of daily fill rates and drainage rates for each hole and correlation coefficient between fill rate and drainage rate for each hole (uncertainty = 1σ; R = Pearson correlation coefficient)

	A		B	
Hole	**Equation**	**r^2**	**Equation**	**r^2**
1	0.00003t-9.8044	0.69	-0.00004t +6.5177	0.67
2	0.00004t+3.5051	0.21	-0.00004t-4.4608	0.22
3	0.0000003t-3.69	0.0039	-0.000002t-3.0366	0.083
4	0.000004t-1.1225	0.24	-0.000001t-4.6633	0.039
5	0.0000003t+4.4844	0.0013	-0.0000004t-3.6435	0.014
6	0.000002t+0.4009	0.244	-0.000001t-1.3274	0.155
7	0.000002t+1.5792	0.054	-0.000001t-3.0762	0.268
8	0.000003t-0.295	0.3284	-0.000004t+0.1086	0.353

Table 4: Equations and linear regression coefficients for the changes in fill rate (A) and drainage rate (B) in each hole over the observation period.

Time (mins)	Hole number					
	1	**2**	**3**	**4**	**5**	**6**
5	-0.157	-1.479	3.78	-4.205	-2.38	-0.379
10	-0.0787	-0.843	2.48	-1.743	-0.924	-0.0283
15	-0.0754	-0.599	0.927	-1.063	-0.640	0.0198
20	0.0628	-0.477	0.498	-0.737	-0.488	0.0177
25	-0.0589	-0.394	0.259	-0.551	-0.366	0.0281
30	-0.0559		0.155	-0.440	-0.285	0.0235
35	-0.0517		0.0961	-0.369	-0.251	0.0233
40	-0.0463		0.0584	-0.320	-0.217	0.0439
45	-0.0382		0.0249	-0.280	-0.188	0.0484
50	-0.0353		0.0181	-0.248	-0.165	0.0483
55	-0.0320		0.00391	-0.222	-0.154	0.0460
60	-0.0294		0.00522	-0.198	-0.135	0.0432
65	-0.0279		0.00180		-0.127	0.0407
70	-0.0271		-0.00139		-0.118	0.0389
K_{av}	-0.0555 ± 0.034	-0.758 ± 0.437	0.554 ± 1.105	-0.865 ± 1.143	-0.294 ± 0.48	0.0055 ± 0.104

Table 5: K (cm hr^{-1}) at 5 minute resolution for slug and bail tests. Uncertainty = 1σ

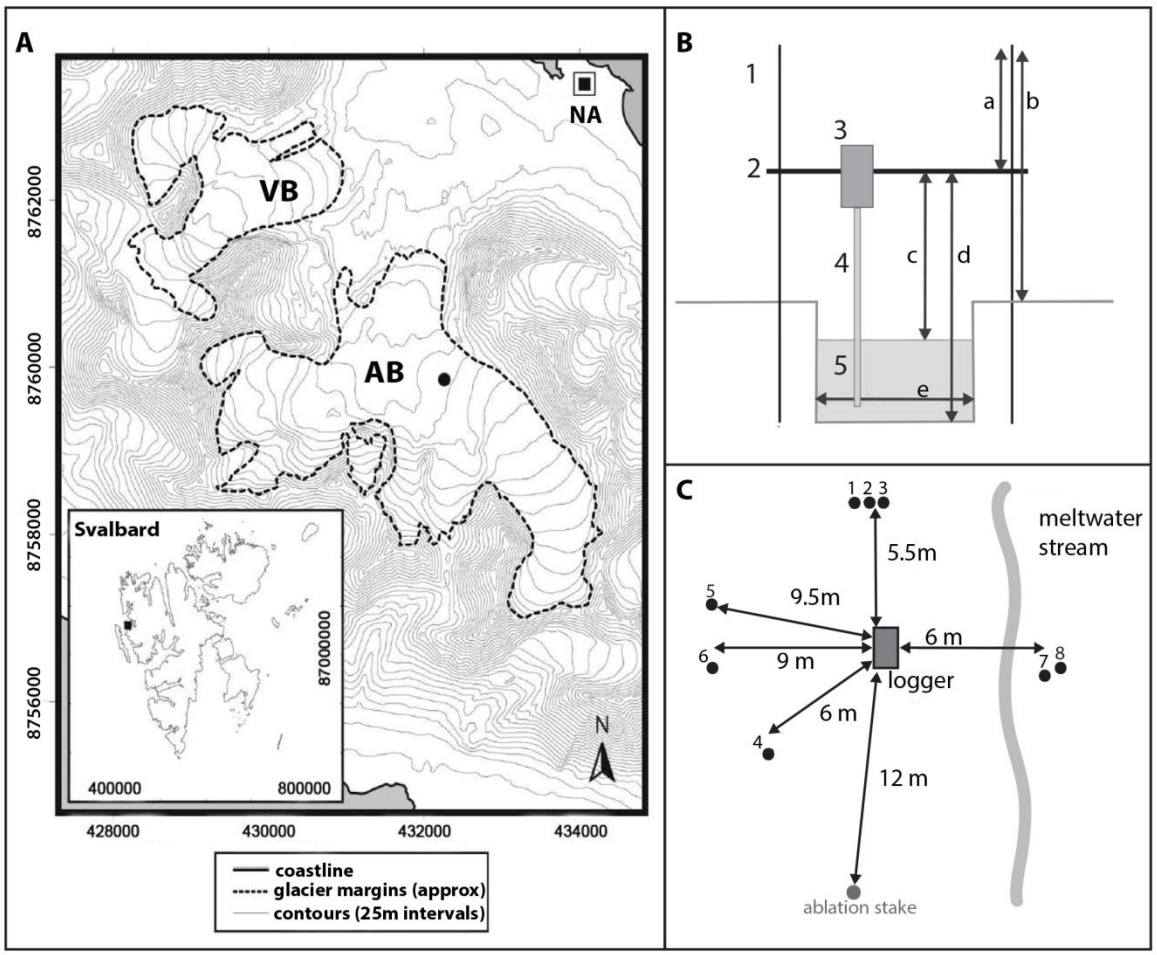

Figure 1 A: map showing the location of Austre Brøggerbreen (AB) and the adjacent Vestre Brøggerbreen (VB), with the nearby town Ny Alesund (NA) also marked. The inset shows the position of these glaciers on the Svalbard archipelago. B: Schematic of the goalpost structure and the associated measurements, where 1 = vertical rig pole, 2 = horizontal crossbar, 3 = water level sensor circuitry, 4 = water level sensor probe, 5 = cryoconite hole water, a = top of rig pole to crossbar, b = top of rig pole to ice surface, c = crossbar to hole water, d = crossbar to hole floor, e = hole width. C: map of field site

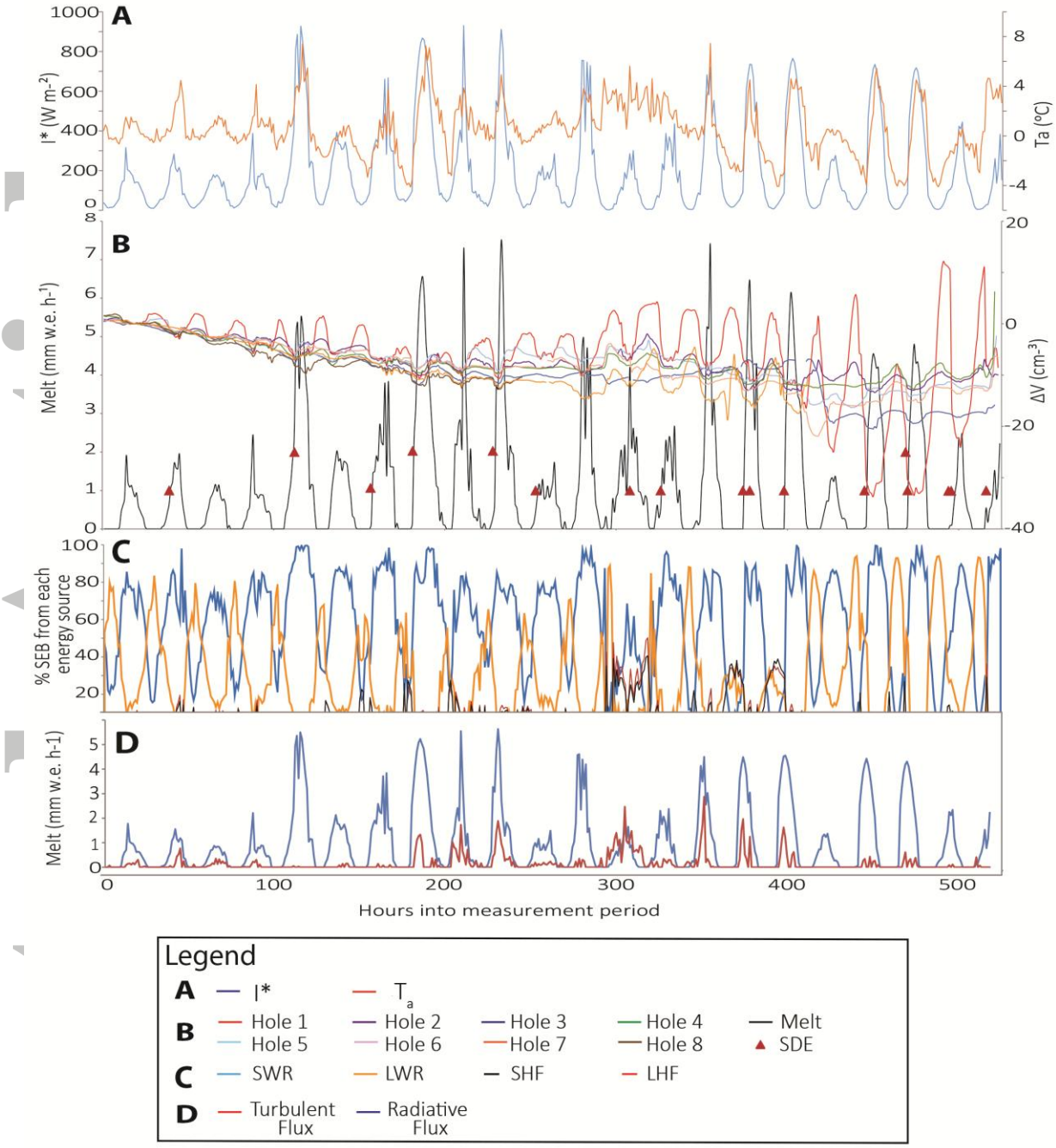

Figure 2: A: I* and Ta over the observation period; B: melt rate, ΔVw and SDEs for all holes over the observation period Raised triangles indicate simultaneous SDEs in two holes. C: The percentage of the total surface energy balance (SEB) attributed to shortwave radiation (SWR), longwave radiation (LWR), sensible heat flux (SHF) and latent heat flux (LHF) throughout the observation period. Radiative fluxes are represented by filled areas whereas turbulent fluxes are represented by lines for clarity; D: Melt attributed to radiative fluxes and turbulent fluxes through the measurement period. The x-axis is shared by all four graphs.

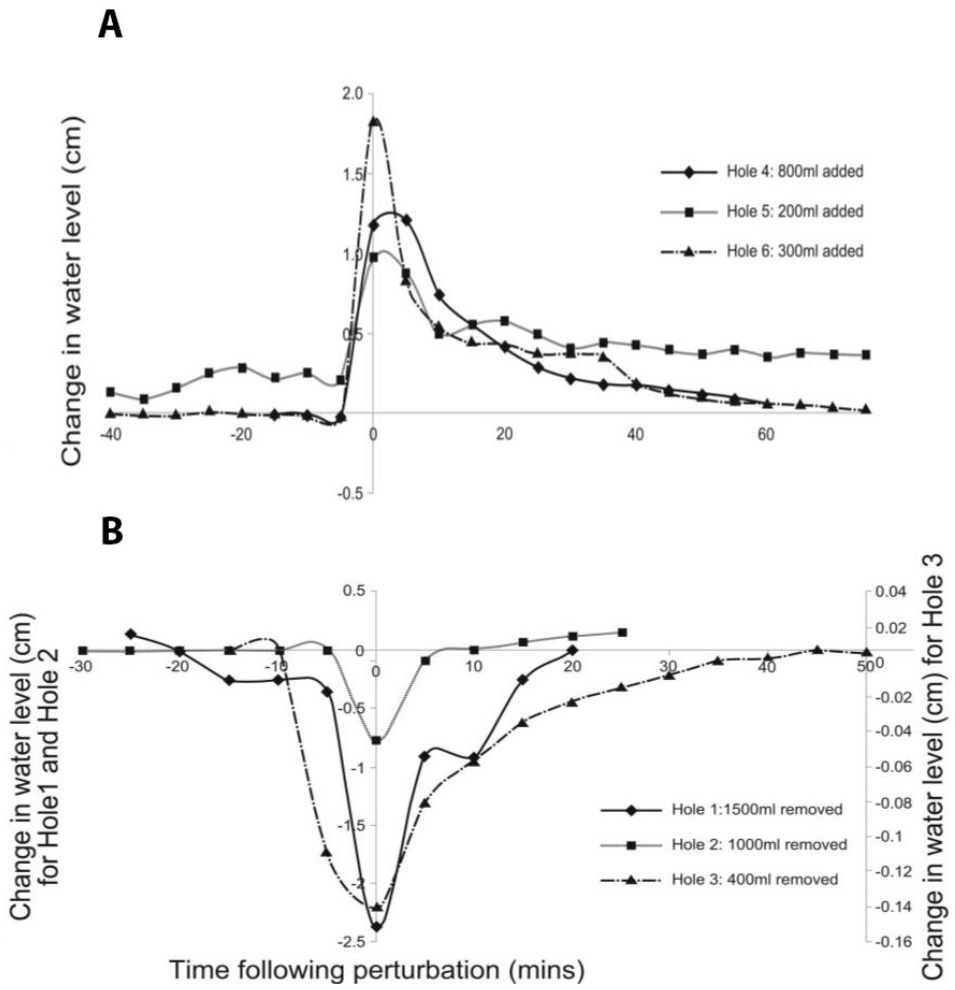

Figure 3 A: Return times for Vw in holes 4 – 6 following slug tests; B: return times for Vw in holes 1-3 following bail tests.